Advances in Water Resources 33 (2010) 640–651

Contents lists available at ScienceDirect

Advances in Water Resources

journal homepage: www.elsevier.com/ locate/advwatres

A new analytical solution solved by triple series equations method for constant-head tests in confined aquifers

Ya-Chi Chang, Hund-Der Yeh *

Institute of Environmental Engineering, National Chiao-Tung University, Hsinchu, Taiwan

ARTICLE INFO

Article history:
Received 21 May 2009
Received in revised form 18 March 2010
Accepted 18 March 2010
Available online 25 March 2010

Keywords:
Constant-head test
Aquifer
Mixed boundary value problem
Partially penetrating well

ABSTRACT

The constant-head pumping tests are usually employed to determine the aquifer parameters and they can be performed in fully or partially penetrating wells. Generally, the Dirichlet condition is prescribed along the well screen and the Neumann type no-flow condition is specified over the unscreened part of the test well. The mathematical model describing the aquifer response to a constant-head test performed in a fully penetrating well can be easily solved by the conventional integral transform technique under the uniform Dirichlet-type condition along the rim of wellbore. However, the boundary condition for a test well with partial penetration should be considered as a mixed-type condition. This mixed boundary value problem in a confined aquifer system of infinite radial extent and finite vertical extent is solved by the Laplace and finite Fourier transforms in conjunction with the triple series equations method. This approach provides analytical results for the drawdown in a partially penetrating well for arbitrary location of the well screen in a finite thickness aquifer. The semi-analytical solutions are particularly useful for the practical applications from the computational point of view.

1. Introduction

Hydraulic parameters such as hydraulic conductivity, specific storage and leakage factor are important for quantifying groundwater resources. To determine these parameters, the constant-head pumping test is generally employed if the aquifer has low permeability. During the test, the hydraulic head at the well is kept constant throughout the test period and the transient flow rate across the wellbore is measured at the same time. A pumping test performed in a fully or partially penetrating borehole is influenced by the well skin effect. The fully penetrating well can be simulated as a Dirichlet (also called the first type) boundary condition, and the relative models can be solved by the conventional integral transform techniques [11]. If the well skin effect is negligible in the model, the Dirichlet and Neumann (second type) boundary conditions are appropriate for describing the drawdown along the well screen and casing, respectively. Thus, the boundary condition along the well face in the partially penetrating well is a mixed-type condition. The term "mixed-type" boundary condition is used to distinguish this boundary condition from the "uniform" Dirichlet and Neumann boundary condition or a combination of Dirichlet and Neumann boundary conditions (which is usually defined as third type or Robin type boundary condition). If the well skin effect is considered in the model, a more appropriate description for such an aquifer system is to treat the skin zone as a different formation zone instead of using a skin factor. Thus, the aquifer system naturally becomes a two-zone formation (see, e.g., [26,27,34,35]).

Mixed boundary conditions are widely used to describe many boundary value problems of mathematical physics. Such problems arise in potential theory and its numerous applications to engineering, fracture mechanics, heat conduction, and many others. Only limited analytical solutions to mixed boundary problems (MBPs) in the field of well hydraulics have been found so far by special solution techniques including the dual integral/series equation [8,22], Weiner–Hopf technique [18], and Green's function [12]. Most of the solutions to MBPs have been obtained numerically [29], or by approximate methods such as asymptotic analysis [2], or perturbation techniques [8,25].

For the mathematical model under the mixed boundary condition in a confined aquifer of semi-infinite thickness, Wilkinson and Hammond [25] used a perturbation method to give an approximate solution for drawdown changes at the well. Cassiani and Kabala [4] used the dual integral equation method to develop a Laplace-domain solution that accounts for the effects of wellbore storage, infinitesimal skin, and aquifer anisotropy. Cassiani et al. [5] further used the same method to develop the solutions in Laplace domain suited for constant-head pumping tests and double packer tests treated as the MBPs. Selim and Kirkham [21] used the Gram–Schmidt orthonormalization method to develop a steady state solution in a confined aquifer of finite horizontal extent. Similar problems under the mixed boundary conditions also arise in the field of heat conduction. Among others, Huang [13] used the Weiner–Hopf technique to develop a solution in a semi-infinite slab and Huang and Chang [12] combined

* Corresponding author. 300 Institute of Environmental Engineering, National Chiao Tung University, 1001 University Road, Hsinchu, Taiwan.
E-mail address: hdyeh@mail.nctu.edu.tw (H.-D. Yeh).

0309-1708/$ – see front matter © 2010 Elsevier Ltd. All rights reserved.
doi:10.1016/j.advwatres.2010.03.010

the Green's function with conformal mapping to develop the solution in an elliptic disk.

In reality, the thickness of aquifer is generally finite. Cassiani et al. [5] have developed the Laplace-domain solutions to MBPs for constant-head test based on the infinite aquifer thickness assumption. Their solutions are appropriate for the early time condition when the pressure change caused by the constant-head pumping has not reached the bottom of the aquifer or for the special condition, where the screen length is significantly shorter than the aquifer thickness. Chang and Chen [6] removed such constraints by assuming finite aquifer thickness and treated the well skin effect as a skin factor. They also treated the boundary along the well screen as a Robin (third type) boundary condition and replaced the mixed boundary by homogeneous Neumann boundary. They considered the wellbore flux entering through the well screen as unknown and discretized the screen length into M segments [7]. To avoid discretizing the well screen, Chang and Yeh [8] developed an analytical solution for a constant-head test performed in a partially penetrating well in an aquifer. They used the dual series equations (DSE) method and perturbation method to solve the MBP along the well which has a well screen extended from the top of the aquifer to any location of the well. According to the image well theory, their solution is applicable to the situation where the middle of the screen of the partially penetrating well is located right at the center of the aquifer. However, their solution can not apply to the case of a partially penetrating well with arbitrary location of the well screen.

This study aims to develop a new model describing a constant-head test performed in a flowing partially penetrating well for arbitrary location of the well screen in an aquifer of a finite thickness in depth. The solution of the model is based on the following assumptions: (1) the aquifer is homogeneous and infinite extent in the radial direction; (2) the well has a finite radius; (3) the initial head is constant and uniform throughout the whole aquifer; and (4) the well loss is not considered in the system. The mixed-type boundary condition at the well is handled via the triple series equations (TSE) method. This solution contains infinite series involving the summations of multiplication of integrals, trigonometric functions, and the modified Bessel functions of second kind, where the single and double integrals are presented in terms of trigonometric functions multiplying the associated Legendre functions. The infinite-series solution is difficult to accurately compute due to the oscillatory nature and slow convergence of the multiplied functions. Therefore, Shanks' transform method [19,20] is used to accelerate the evaluation of the Laplace-domain solution and the numerical inversion scheme, Stehfest algorithm [24], is used to find the time domain solution. To the best of our knowledge, this is the first paper using the TSE method to solve the mixed boundary value problems in the area of water resources.

2. Mathematical model

2.1. Mathematical statement

Fig. 1 shows a schematic representation of a partially penetrating well in a confined aquifer with a finite thickness of b. The drawdown at the distance r from the well and the distance z from the bottom of the aquifer at time t is denoted as $s(r, z, t)$. The well screen which extends from arbitrary location d_1 to d_2 is of length l under a prescribed constant drawdown h_w. The hydraulic parameters of the aquifer are horizontal hydraulic conductivity K_r [L/T], vertical hydraulic conductivity K_z [L/T], and specific storage S_s [1/L]. The governing equation for the drawdown can be written as

$$K_r\left(\frac{\partial^2 s}{\partial r^2}+\frac{1}{r}\frac{\partial s}{\partial r}\right)+K_z\frac{\partial^2 s}{\partial z^2}=S_s\frac{\partial s}{\partial t}. \tag{1}$$

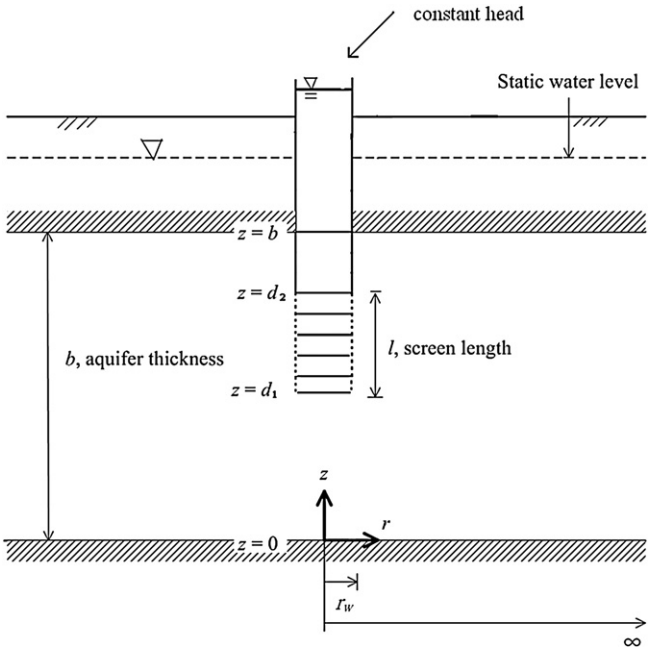

Fig. 1. Schematic representation of a partially penetrating well in a confined aquifer of finite extent with a finite thickness of b.

The prescribed Dirichlet boundary condition for a constant drawdown along the well screen is:

$$s(r_w,z,t)=s_w \quad d_1\le z\le d_2\,. \tag{2a}$$

A Neumann boundary condition of zero flux is specified as:

$$\left.\frac{\partial s}{\partial r}\right|_{r=r_w}=0 \quad 0\le z\le d_1 \quad \text{and} \quad d_2\le z\le b. \tag{2b}$$

In addition, the initial condition and other boundary conditions are:

$$s(r,z,0)=0 \tag{3}$$

$$s(\infty,z,t)=0 \tag{4}$$

and

$$\frac{\partial s}{\partial z}=0,\quad z=0,z=b. \tag{5}$$

The dimensionless parameters used hereafter are defined in Table 1. Eqs. (1)–(5) in dimensionless form are, respectively,

$$\frac{\partial^2 s^*}{\partial \rho^2}+\frac{1}{\rho}\frac{\partial s^*}{\partial \rho}+\alpha^2\frac{\partial^2 s^*}{\partial \xi^2}=\frac{\partial s^*}{\partial \tau} \tag{6}$$

$$s^*(\rho,\xi,\tau=0)=0 \tag{7}$$

$$s^*(\rho=\infty,\xi,\tau)=0 \tag{8}$$

$$s^*(\rho=1,\xi,\tau)=1, \qquad \xi_1\le\xi\le\xi_2 \tag{9a}$$

$$\left.\frac{\partial s^*}{\partial \rho}\right|_{\rho=1}=0, \qquad 0\le\xi\le\xi_1 \quad \text{and} \quad \xi_2\le\xi\le\beta \tag{9b}$$

$$\left.\frac{\partial s^*}{\partial \xi}\right|_{\xi=0,\xi=\beta}=0. \tag{10}$$

Note that Eqs. (6)–(10) constitute a MBP.

Table 1
Dimensionless expressions.

Symbol	Illustration
$s^*(\rho, \xi, \tau)$	$s(r, z, t)/s_w$, dimensionless drawdown
$\bar{s}^*(\rho, \xi, \tau)$	Dimensionless drawdown in Laplace domain
$\bar{\tilde{s}}^*(\rho, \xi, \tau)$	Dimensionless drawdown in Laplace and Fourier domain
α	$\sqrt{K_z / K_r}$, anisotropy ratio
β	b/r_w, dimensionless aquifer thickness
η_n	$n\pi/\beta$
ρ	r/r_w, dimensionless radial distance
τ	$K_r t/S_s r_w^2$, dimensionless time
λ	l/r_w, dimensionless screen length
λ_n	$\sqrt{(n\pi\alpha/\beta)^2 + p}$
ξ	z/r_w, dimensionless vertical distance
ξ_1	d_1/r_w
ξ_2	d_2/r_w
ω	l/b, partial penetration ratio

2.2. Laplace-domain solution

The detailed derivation for the solution of Eq. (6) with Eqs. (7)–(10) using Laplace transform, finite Fourier cosine transform, and TSE method is given in Appendix A. The solution for drawdown in an aquifer involving a partially penetrating well is obtained as:

$$\bar{s}^*(\rho, \xi, p) = \frac{1}{2} B(0,p) \frac{K_0(\sqrt{p}\rho)}{K_0(\sqrt{p})} + \sum_{n=1}^{\infty} B(n,p) \frac{K_0(\lambda_n \rho)}{K_0(\lambda_n)} \cos(\eta_n \xi) \quad (11)$$

where K_0 is the modified Bessel functions of the second kind with order zero, $\eta_n = (n\pi)/\beta$ and the coefficients $B(0, p)$ and $B(n, p)$ are expressed as

$$\begin{aligned} B(0,p) &= C(0,p) + D(0,p) \\ &= C_0 + D_0 \\ &= B_0 \end{aligned} \quad (12)$$

and

$$\begin{aligned} B(n,p) &= C(n,p) + D(n,p) \\ &= C_n + D_n \\ &= B_n. \end{aligned} \quad (13)$$

The coefficients C_0, C_n, D_0, and D_n in Eqs. (12) and (13) are calculated by the following equations

$$C_0 = (1 + \sqrt{p} H_0 \Omega_1(\mu_1))^{-1} \left[\frac{4}{p\pi} \Omega_3(\mu_1) + \frac{2}{p}\left(1 - \frac{\mu_1}{\pi}\right) + \sum_{k=1}^{\infty} \frac{2}{k} (I_k C_k - \lambda_k H_k D_k) \Omega_2(\mu_1, k) - D_0 \sqrt{p} H_0 \Omega_1(\mu_1) \right] \quad (14)$$

$$\begin{aligned} C_n = {} & \sum_{k=1}^{\infty} \frac{1}{k} (I_k C_k - \lambda_k H_k D_k) \left[\Omega_2(\mu_1, k) f_2(n, \mu_1) - \int_0^{\mu_1} \Omega_2(y,k) \frac{df_2(n,y)}{dy} dy \right] \\ & + \frac{1}{2} \sqrt{p} H_0 (C_0 + D_0) \left[\int_0^{\mu_1} \Omega_1(y) \frac{df_2(n,y)}{dy} dy - \Omega_1(\mu_1) f_2(n, \mu_1) \right] \\ & + \frac{2}{p\pi} \left[\Omega_3(\mu_1) f_2(n, \mu_1) - \int_0^{\mu_1} \Omega_3(y) \frac{df_2(n,y)}{dy} dy \right] \\ & - \frac{2 \sin(n\mu_1)}{p n \pi} \end{aligned} \quad (15)$$

$$D_0 = (1 + \sqrt{p} H_0 \Omega_1(\mu_2))^{-1} \left[\sum_{k=1}^{\infty} \frac{2}{k} (-1)^k \Omega_2(\mu_2, k) (I_k D_k - \lambda_k H_k C_k) - C_0 \sqrt{p} H_0 \Omega_1(\mu_2) \right] \quad (16)$$

and

$$\begin{aligned} D_n = {} & (-1)^n \sum_{k=1}^{\infty} (-1)^k \frac{1}{k} (I_k D_k - \lambda_k H_k C_k) \\ & \times \left[\Omega_2(\mu_2, k) \cdot f_2(n, \mu_2) - \int_0^{\mu_2} \Omega_2(y,k) \frac{df_2(n,y)}{dy} dy \right] \\ & + \frac{1}{2} \sqrt{p} H_0 (D_0 + C_0) \left[\int_0^{\mu_2} \Omega_1(y) \frac{df_2(n,y)}{dy} dy - \Omega_1(\mu_2) f_2(n, \mu_2) \right] \end{aligned} \quad (17)$$

with

$$\mu_1 = \xi_1 \pi / \beta \quad (18)$$

$$\mu_2 = (\pi - \xi_2 \pi / \beta) \quad (19)$$

$$\Omega_1(x) = \int_0^x f_1(u,x) u du \quad (20)$$

$$\Omega_2(x,k) = \int_0^x f_1(u,x) \sin(ku) du \quad (21)$$

$$\Omega_3(x) = \int_0^x f_1(u,x) f_3(u,x) du \quad (22)$$

$$\lambda_n = \sqrt{\left(\frac{n\pi\alpha}{\beta}\right)^2 + p} \quad (23)$$

$$H(n,p) = H_n = K_1(\lambda_n) / K_0(\lambda_n) \quad (24)$$

$$f_1(x,a) = \frac{\sqrt{2} \sin(x/2)}{\pi \sqrt{\cos(x) - \cos(a)}} \quad (25)$$

$$f_2(n,a) = [P_n(\cos a) + P_{n-1}(\cos a)] \quad (26)$$

$$f_3(x,a) = \frac{1}{4} (\ln(1 - \cos(a + x)) - \ln(1 - \cos(a - x))) \quad (27)$$

where $P_n(\cos(\cdot))$ is the associated Legendre function ([1], p. 335) and K_1 is the modified Bessel functions of the second kind with order one. The definitions of functions or variables used in equations above are also listed in Table 2.

The determination of the values of C_0, C_n, D_0, and D_n in Eqs. (14)–(17) from Eqs. (A29) to (A48) is described in detail in Appendix A. The coefficients B_0 and B_n in the drawdown solution (11) can therefore be determined based on Eqs. (12) and (13).

The flux entering the well screen and the total well discharge obtained using Eq. (11) are respectively given as:

$$\begin{aligned} \bar{q}^*(1, \xi, p) = -\left. \frac{\partial \bar{s}^*(\rho, \xi, p)}{\partial \rho} \right|_{\rho=1} = {} & \frac{1}{2} B_0 \sqrt{p} \frac{K_1(\sqrt{p})}{K_0(\sqrt{p})} \\ & + \sum_{n=1}^{\infty} B_n \lambda_n \frac{K_1(\lambda_n)}{K_0(\lambda_n)} \cos\left(n \frac{\xi}{\beta} \pi\right) \end{aligned} \quad (28)$$

Table 2
Symbol definitions.

Symbol	Illustration
$f_1(x, a)$	$\frac{\sqrt{2}\sin(x/2)}{\pi\sqrt{\cos(x) - \cos(a)}}$
$f_2(n, a)$	$[P_n(\cos a) + P_{n-1}(\cos a)]$, $n \geq 1$
$f_3(x, a)$	$\frac{1}{4}(\ln(1 - \cos(a + x)) - \ln(1 - \cos(a - x)))$
H_n	$K_1(\lambda_n)/K_0(\lambda_n)$
I_n	$n - \lambda_n H_n$
μ_1	$\xi_1 \pi/\beta$
μ_2	$\pi - \xi_2 \pi/\beta$
$\Omega_1(x)$	$\int_0^x f_1(u,x) u du$
$\Omega_2(x, k)$	$\int_0^x f_1(u,x) \sin(ku) du$
$\Omega_3(x)$	$\int_0^x f_1(u,x) f_3(u,x) du$

and

$$Q(p) = \frac{1}{\lambda}\int_{\xi_1}^{\xi_2} \bar{q}^*(1,\xi,p)\mathrm{d}\xi = \frac{1}{2}B_0\sqrt{p}\frac{K_1(\sqrt{p})}{K_0(\sqrt{p})} - \sum_{n=1}^{\infty}(\lambda\eta_n)^{-1}B_n\lambda_n H_n\left[\sin(n\mu_1) + (-1)^n\sin(n\mu_2)\right] \tag{29}$$

where $\lambda = l/r_w$ is the dimensionless length of the screen.

2.3. Simplified solutions

2.3.1. Partially penetrating well (well screen extends from the top of the aquifer)

When the well screen extends from d_1 to the top of the aquifer, the coefficients in Eqs. (14)–(17) can be found by setting $\xi_2 = \beta$. The drawdown can then be determined from solving Eqs. (A17a) and (A17b) which should be identical to the results obtained using infinity-order perturbation approach in solving DSE in Chang and Yeh [8].

2.3.2. Fully penetrating well

When the well fully penetrates the entire thickness of the formation, i.e., ξ_1 is zero and ξ_2 equals β, the drawdown and the well discharge can be obtained using Eqs. (11) and (29), respectively, as [11]

$$\bar{s}^*(\rho,\xi,p) = \frac{1}{p}\frac{K_0(\sqrt{p}\rho)}{K_0(\sqrt{p})} \tag{30}$$

and

$$Q(p) = \frac{K_1(\sqrt{p})}{\sqrt{p}K_0(\sqrt{p})} \tag{31}$$

Eqs. (30) and (31) are identical to the solutions of drawdown and flow rate in Laplace domain given in Yang and Yeh [28].

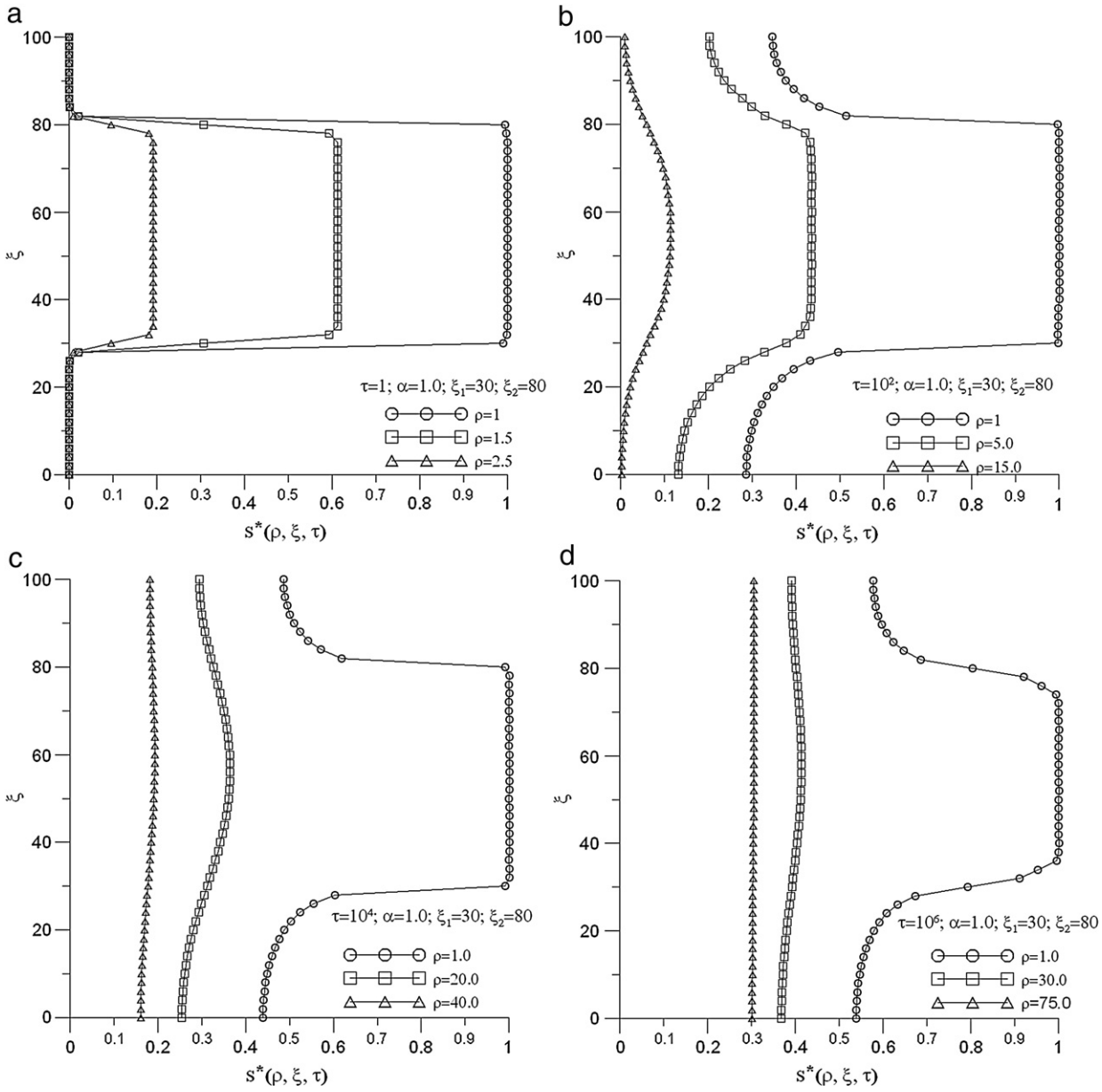

Fig. 2. The drawdown distribution at dimensionless time $\tau = 1$, 100, 10^4 and $\tau = 10^6$ for $\beta = 100$ and various ρ.

3. Results and discussion

Numerical calculations for the aquifer drawdown and well flux are performed in PC using the FORTRAN code developed based on the present solutions. The first step in the development of solutions is to determine the coefficients of Laplace-domain solution in Eq. (11) from using Eq. (A50). The single and double integrals involved in the elements are then computed using the subroutines DQDAG and DTWODQ in IMSL [10,15], respectively. Once the coefficients are known, the second step is to find the infinite summation in Eq. (11) by Shank's transform method. Then the final step is to transform the Laplace-domain solution of Eq. (11) into time-domain using IMSL subroutine LINV for the Stehfest method [24] with eight weighting factors. The infinite summation in the solution can be found more efficiently using Shank's transform which consists of a family of nonlinear sequence-to-sequence transformations [20]. Shanks [20] concluded that these transformations are effective when applied to accelerate the convergence of some slowly convergent sequences and may also converge to some divergent sequences.

The solutions can be verified by calculating the values at the boundary along the test well in Eq. (11). Fig. 2 shows the dimensionless drawdown for $\beta=100$, $\xi_1=30$, $\xi_2=80$ and various ρ at $\tau=1, 100, 10^4$ and 10^6. As indicated in the figure, the dimensionless drawdown is constant along the well screen and decreases with the increasing dimensionless radial distance at $\tau=1$. In addition, the dimensionless drawdown increases with dimensionless time along the unscreened part of the well. The dimensionless drawdown has larger value in the screen part and smaller value along the unscreened part. Fig. 3 shows the plots of the flux along the well screen for $\beta=100$, $\xi_1=30$ and $\xi_2=80$ at $\tau=1$, 100, 10^4 and 10^6. The dimensionless flux is non-uniformly distributed and large at the screen edge due to the vertical flow induced by the presence of well partial penetration. Fig. 4 exhibits the behavior of dimensionless drawdown versus dimensionless time τ and illustrates the effect of screen length on the drawdown response, where the dimensionless radial distance ρ is 10, the vertical distance ξ is 50 and $\alpha=1$ for different length of the screen. This figure indicates that the dimensionless drawdown increases with the length of the screen. To test the influence of anisotropy of the aquifer, Fig. 5 is plotted for $\rho=5$, $\xi=50$, $\xi_1=40$, $\xi_2=60$ and various anisotropy α. As can be observed, the drawdown increases with α. The spatial dimensionless drawdown contours at $\tau=100$, 10^3 and 10^4 are plotted in Fig. 6. The dimensionless drawdown increases with dimensionless time at a fixed radial distance and flow is horizontal when the dimensionless radial distance is large than 80 and the dimensionless time is 10^4. Fig. 7(a) and (b) shows the spatial dimensionless drawdown contours for various α^2 with $\xi_1=200$ and $\xi_2=250$ at $\tau=10^5$ and demonstrates the influence of anisotropy on the dimensionless drawdown. The flow is almost horizontal at the bottom of the aquifer when the dimensionless radial distance is large than 400 for $\alpha^2=1$; however, the flow is vertical at the bottom of the aquifer for $\alpha^2=0.5$. Fig. 8(a) and (b) plots the spatial dimensionless drawdown contours for the same length of 50 but different locations of well screen. In Fig. 8(a), the screen is symmetric with $\xi_1=12.5$ and $\xi_2=37.5$ and in Fig. 8(b) the screen extends from the top of the aquifer with $\xi_1=25$ and $\xi_2=50$ at $\tau=10^5$. Since the screen is symmetric about the middle line of the aquifer, the drawdown contours are symmetric as shown in Fig. 6(a). Fig. 9 illustrates the spatial dimensionless drawdown contours for $\beta=200$, $\xi_1=100$ and $\xi_2=150$ at $\tau=10^7$. The direction of flow is upward when the radial distance is far from the pumping well and it is downward when the radial distance is close to the well screen.

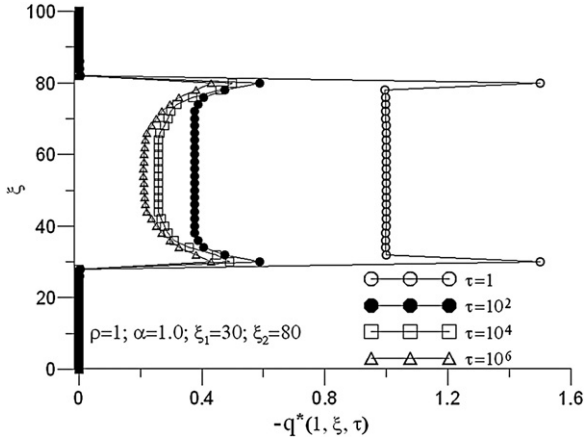

Fig. 3. The distribution of flux along the well screen at different dimensionless time for $\beta=100$.

4. Concluding remarks

This paper developed a new semi-analytical solution for describing the drawdown response for a constant-head test performed in a partially penetrating well in an aquifer of infinite radial extent and finite vertical extent, where the well screen is installed within any part of the well. The Laplace and finite cosine Fourier transforms in conjunction with TSE method are used to solve the mixed-type boundary and initial values problem for a partially penetrating well in an aquifer of a finite thickness. The present solutions can be reduced to the solutions given in Yang and Yeh [28] for a fully penetrating well in an aquifer of a finite thickness. In addition, they are also equal to the results obtained using infinity-order perturbation approach for a partially penetrating well of a well screen extending from the top of the aquifer presented in Chang and Yeh [8]. The flux estimated from the solution is non-uniformly distributed along the screen and with a local peak at the edge, due to the vertical flow induced by the effect of well partial penetration.

These solutions are particularly useful for practical applications since they can be used to evaluate the sensitivities of the input parameters in a mathematical model (e.g., [14] and [9]), to identify the hydraulic parameters if coupling with the extended Kalman filter (e.g., [16] and [33]) or an optimization approach such as the nonlinear least-squares (e.g., [30] and [31]) or simulated annealing (e.g., [17] and [32]) in the analysis of aquifer data, and to validate a numerical solution [36].

Acknowledgements

This study was supported by the Taiwan National Science Council under the grant NSC 96-2221-E-009-087-MY3. The authors would like to thank three anonymous reviewers for their valuable and constructive comments that help improve the clarity of our presentation.

Appendix A

The Laplace-domain solution for dimensionless drawdown can be obtained by taking the Laplace transform with respect to time and the finite Fourier cosine transform with respect to ξ. The definition of Laplace transform is:

$$\bar{s}^*(\rho,\xi,p)=L_p[s^*(\rho,\xi,\tau);\tau\to p]=\int_0^\infty s^*(\rho,\xi,\tau)e^{-p\tau}d\tau \qquad (A1)$$

where $\bar{s}^*(\rho, \xi, p)$ is the dimensionless drawdown in Laplace domain.

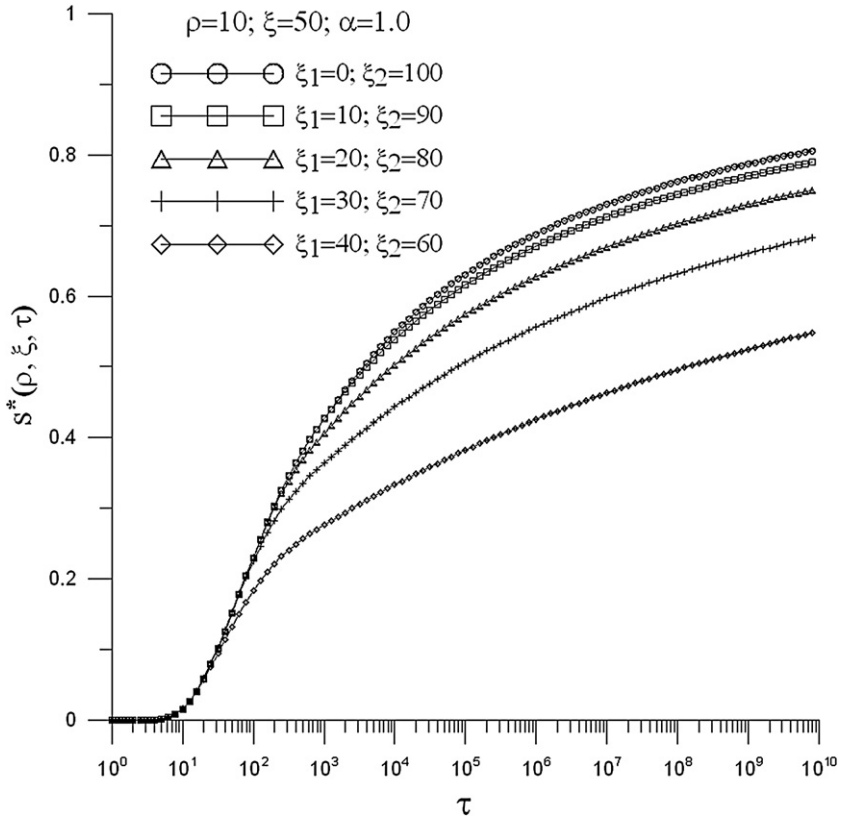

Fig. 4. Type curve for drawdown for $\rho = 10$, $\xi = 50$, $\alpha = 1$, $\beta = 100$ and various penetration lengths.

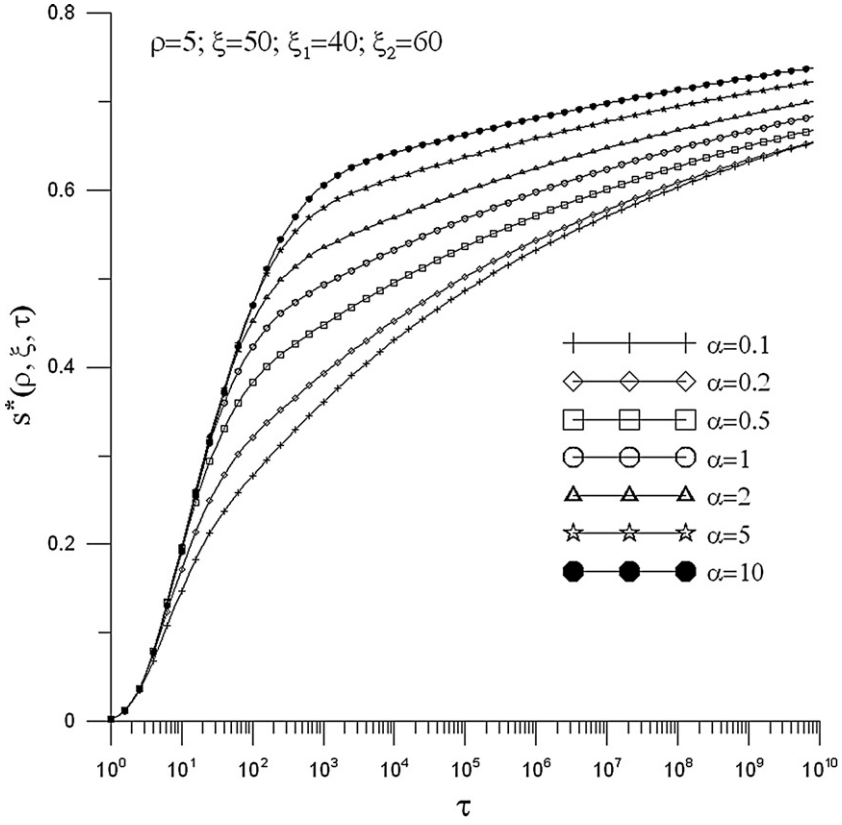

Fig. 5. Type curve for drawdown for $\rho = 5$, $\xi_1 = 40$, $\xi_2 = 60$, $\beta = 100$ and various anisotropy α.

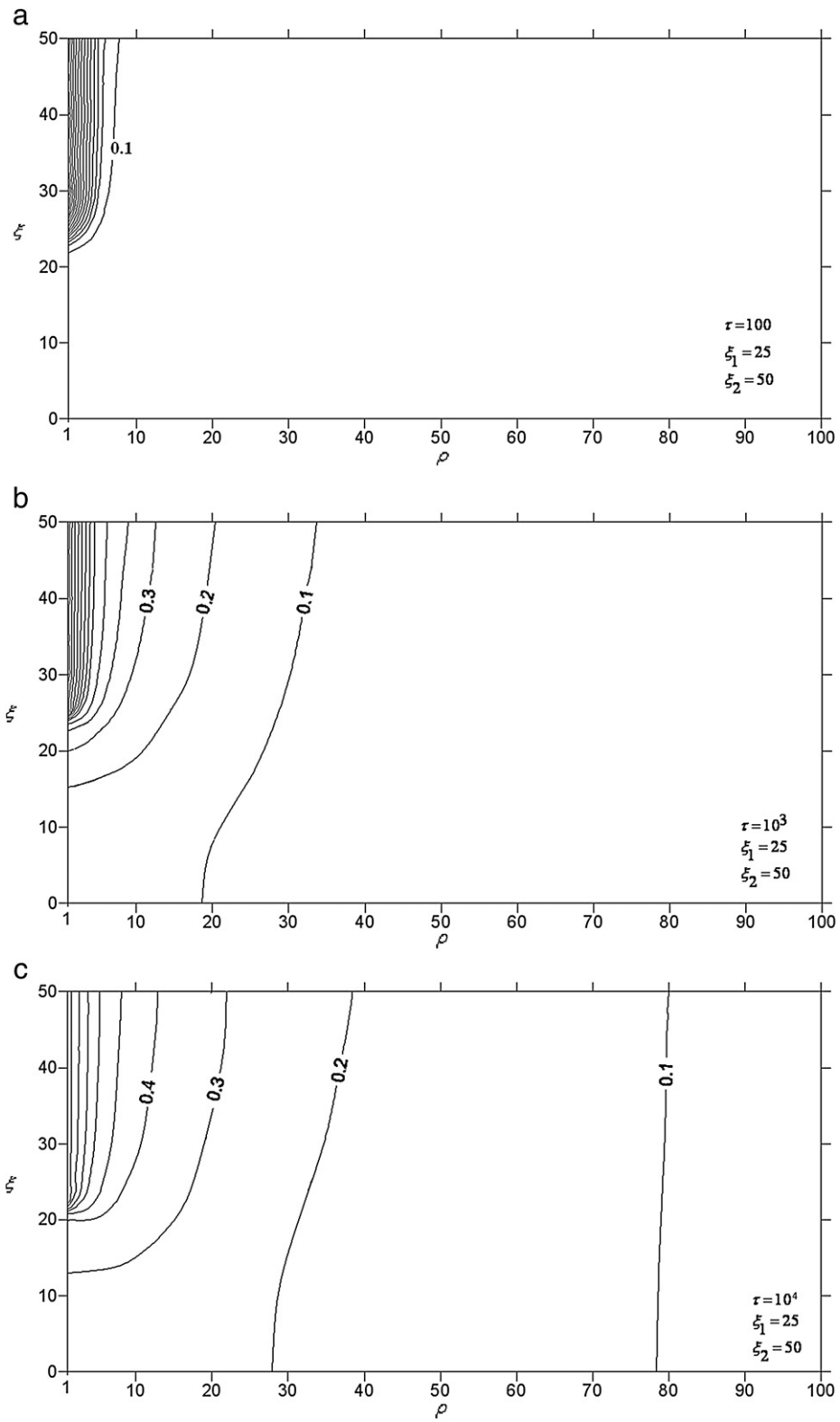

Fig. 6. The spatial drawdown contours at dimensionless time $\tau = 100$, 10^3 and $\tau = 10^4$ for $\beta = 50$.

Taking the Laplace transform of Eq. (6) and Eqs. (8)–(10) with the initial condition in Eq. (7), the problem reads:

$$\frac{\partial^2 \bar{s}^*}{\partial \rho^2} + \frac{1}{\rho}\frac{\partial \bar{s}^*}{\partial \rho} + \alpha^2 \frac{\partial^2 \bar{s}^*}{\partial \xi^2} - p\bar{s}^* = 0 \tag{A2}$$

$$\bar{s}^*(\rho = \infty, \xi, p) = 0 \tag{A3}$$

$$\bar{s}^*(\rho = 1, \xi, p) = \frac{1}{p}, \quad \xi_1 \le \xi \le \xi_2 \tag{A4a}$$

$$\left.\frac{\partial \bar{s}^*}{\partial \rho}\right|_{\rho=1} = 0, \quad 0 \le \xi \le \xi_1 \quad \text{and} \quad \xi_2 \le \xi \le \beta \tag{A4b}$$

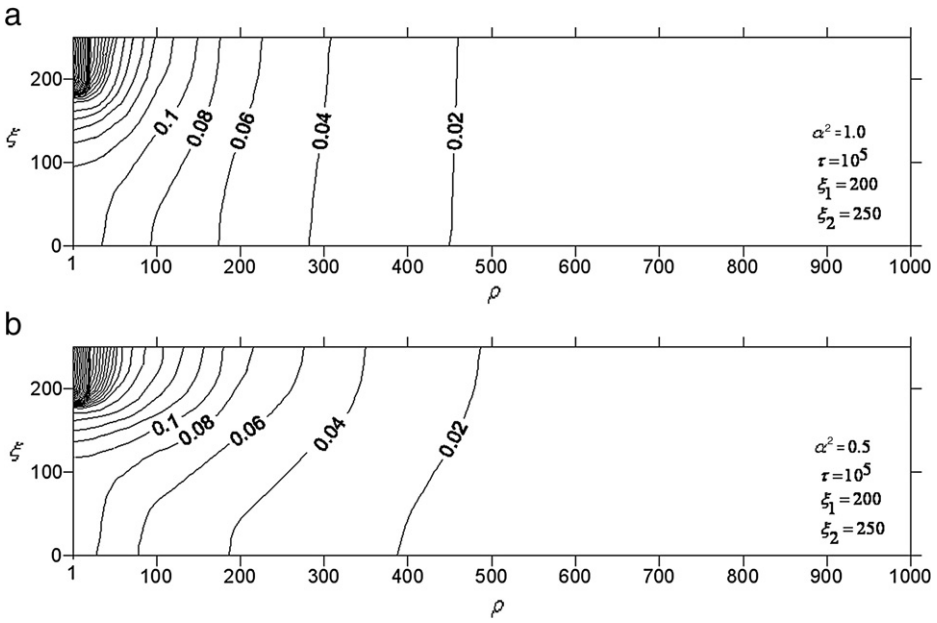

Fig. 7. The spatial drawdown contours at dimensionless time $\tau = 10^5$ for $\beta = 250$ and various α^2.

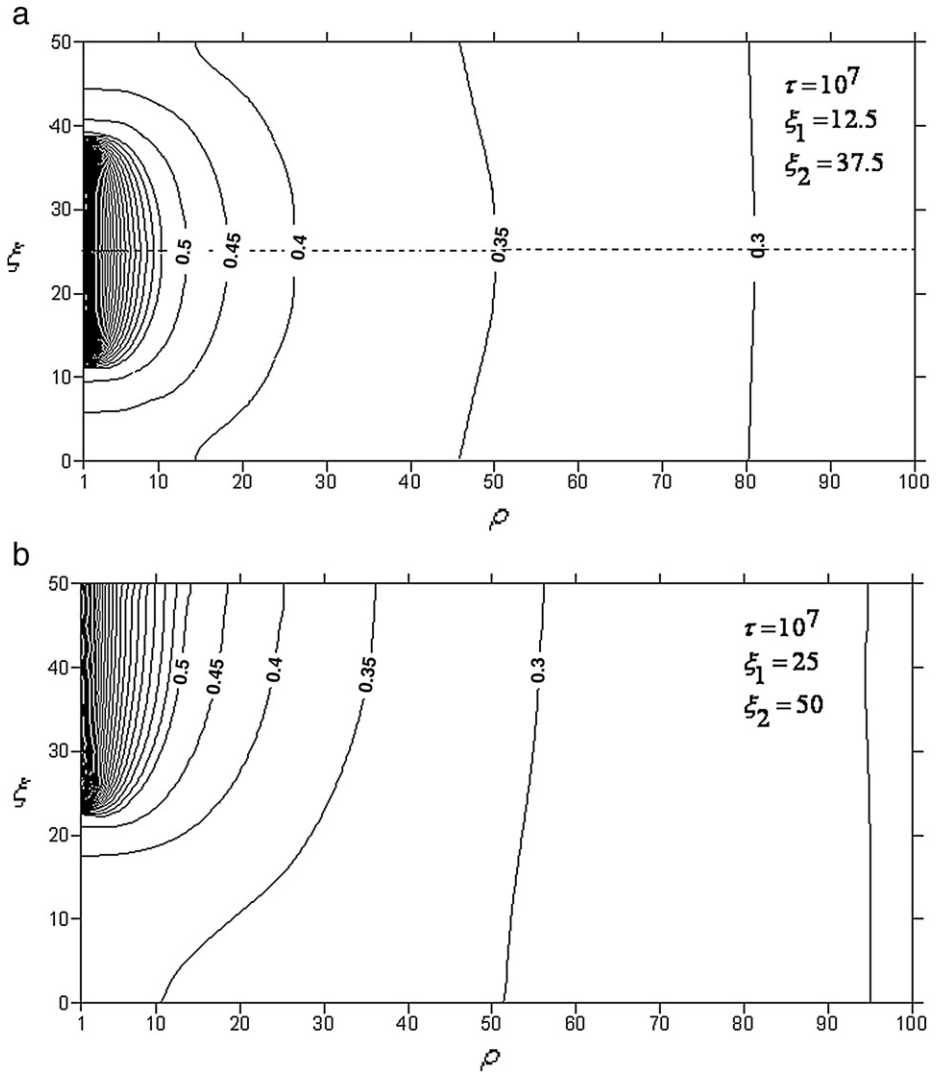

Fig. 8. The spatial drawdown contours at dimensionless time $\tau = 10^6$ for $\beta = 50$ and various screen locations ($\xi_1 = 12.5$ and $\xi_2 = 37.5$; $\xi_1 = 25$ and $\xi_2 = 50$).

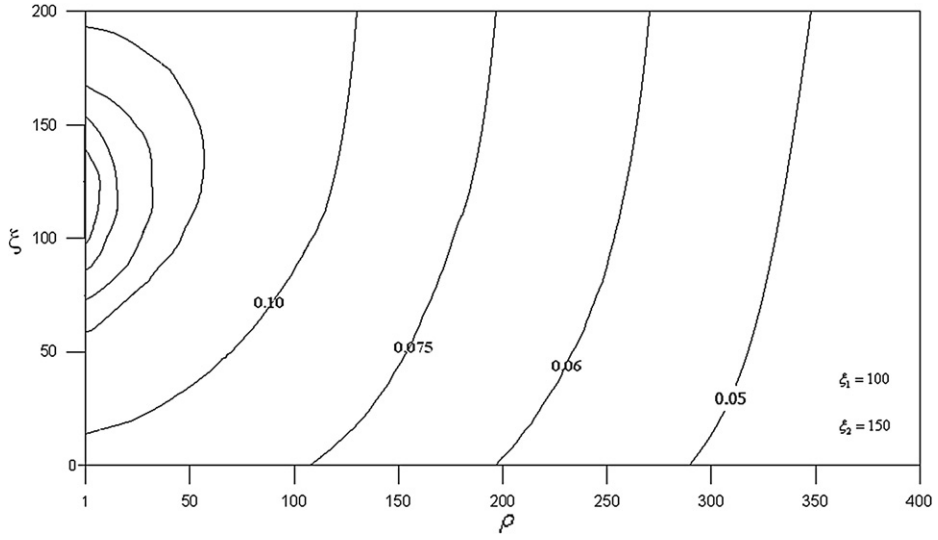

Fig. 9. The spatial drawdown contours as at dimensionless time $\tau = 10^7$ for $\beta = 200$, $\xi_1 = 100$ and $\xi_2 = 150$.

$$\left.\frac{\partial \bar{s}^*}{\partial \xi}\right|_{\xi=0,\xi=\beta} = 0 \tag{A5}$$

The finite cosine Fourier transform with respect to ξ is then defined as follows [23]:

$$\hat{\bar{s}}^*(\rho,n,p) = F_c[\bar{s}^*(\rho,\xi,p);\xi\rightarrow n] = \int_0^\beta \bar{s}^*(\rho,\xi,p)\cos(\eta_n\xi)d\xi \tag{A6}$$

where $\hat{\bar{s}}^*(\rho,n,p)$ is the dimensionless drawdown after finite cosine Fourier transform. Substituting Eq. (A6) into Eqs. (A2), (A3) and (A5) results in the Bessel differential equation as

$$\frac{\partial^2 \hat{\bar{s}}^*}{\partial\rho^2} + \frac{1}{\rho}\frac{\partial \hat{\bar{s}}^*}{\partial\rho} - \lambda_n^2 \hat{\bar{s}}^* = 0 \tag{A7}$$

with the boundary condition

$$\hat{\bar{s}}^*(\rho=\infty,n,p) = 0. \tag{A8}$$

The general solution to Eq. (A7) with the boundary condition (A8) is [3]

$$\hat{\bar{s}}^*(\rho,n,p) = A(n,p)K_0(\lambda_n\rho) \tag{A9}$$

where $A(n, p)$ can be found from using the mixed-type boundary condition (A4a) and (A4b). The inverse of the finite cosine Fourier transform is

$$\bar{s}^*(\rho,\xi,p) = \frac{1}{\beta}\hat{\bar{s}}^*(\rho,0,p) + \frac{2}{\beta}\sum_{n=1}^{\infty}\hat{\bar{s}}^*(\rho,n,p)\cos(\eta_n\xi). \tag{A10}$$

Thus, the solution in ξ domain obtained by inserting Eq. (A9) into Eq. (A10) is

$$\bar{s}^*(\rho,\xi,p) = \frac{1}{\beta}A(0,p)K_0(\sqrt{p}\rho) + \frac{2}{\beta}\sum_{n=1}^{\infty}A(n,p)K_0(\lambda_n\rho)\cos(\eta_n\xi) \tag{A11}$$

with its derivative with respect to ρ given by

$$\frac{\partial \bar{s}^*}{\partial\rho}(\rho,\xi,p) = -\frac{1}{\beta}A(0,p)\sqrt{p}K_1(\sqrt{p}\rho) - \frac{2}{\beta}\sum_{n=1}^{\infty}A(n,p)\lambda_n K_1(\lambda_n\rho)\cos(\eta_n\xi). \tag{A12}$$

Substituting Eq. (A11) into Eqs. (A4a) and (A12) into Eq. (A4b) results in a system of TSE as

$$\frac{1}{\beta}A(0,p)K_0(\sqrt{p}) + \frac{2}{\beta}\sum_{n=1}^{\infty}A(n,p)K_0(\lambda_n)\cos(\eta_n\xi) = \frac{1}{p}, \quad \xi_1\le\xi\le\xi_2 \tag{A13a}$$

$$\frac{1}{\beta}A(0,p)\sqrt{p}K_1(\sqrt{p}) + \frac{2}{\beta}\sum_{n=1}^{\infty}A(n,p)\lambda_n K_1(\lambda_n)\cos(\eta_n\xi) = 0, \quad 0\le\xi\le\xi_1, \quad \xi_2\le\xi\le\beta. \tag{A13b}$$

Introduce

$$B(n,p) = 2A(n,p)K_0(\lambda_n)/\beta \tag{A14}$$

and

$$x = \xi\pi/\beta. \tag{A15}$$

Therefore, $\eta_n\xi = nx$ and the TSE of Eqs. (A13a) and (A13b) can be rearranged as [22]:

$$\frac{1}{2}B(0,p)\sqrt{p}H(0,p) + \sum_{n=1}^{\infty}B(n,p)\lambda_n H_n\cos(nx) = 0, \quad 0\le x\le\frac{\xi_1}{\beta}\pi \tag{A16a}$$

$$\frac{1}{2}B(0,p) + \sum_{n=1}^{\infty}B(n,p)\cos(nx) = \frac{1}{p}, \quad \frac{\xi_1}{\beta}\pi < x \le \frac{\xi_2}{\beta}\pi \tag{A16b}$$

$$\frac{1}{2}B(0,p)\sqrt{p}H(0,p) + \sum_{n=1}^{\infty}B(n,p)\lambda_n H_n\cos(nx) = 0, \quad \frac{\xi_2}{\beta}\pi\le x\le\pi. \tag{A16c}$$

The symbol H_n is defined in Eq. (24) and H_0 is from H_n when $n = 0$. Our goal now is to determine the coefficients $B(0, p)$ and $B(n, p)$ in Eqs. (A16a)–(A16c). For convenience, the coefficients $B(0,p)$ and $B(n,p)$ are expressed as B_0 and B_n, respectively, as in Eqs. (12) and (13). To solve

the TSE in Eq. (A16a)–(A16c), we further split it into the following two DSE ([22], p. 192)

$$\frac{1}{2}(C_0+D_0)\sqrt{p}H(0,p)+\sum_{n=1}^{\infty}(C_n+D_n)\lambda_n H_n\cos(nx)=0,\qquad 0\le x\le\mu_1 \tag{A17a}$$

$$\frac{1}{2}C_0+\sum_{n=1}^{\infty}C_n\cos(nx)=\frac{1}{p},\qquad \mu_1<x\le\pi \tag{A17b}$$

$$\frac{1}{2}D_0+\sum_{n=1}^{\infty}D_n\cos(nx)=0,\qquad 0<x\le\pi-\mu_2 \tag{A18a}$$

$$\frac{1}{2}(C_0+D_0)\sqrt{p}H(0,p)+\sum_{n=1}^{\infty}(C_n+D_n)\lambda_n H_n\cos(nx)=0,\qquad \pi-\mu_2\le x\le\pi \tag{A18b}$$

where μ_1 and μ_2 are defined by Eqs. (18) and (19), respectively. With Eqs. (12) and (13), Eqs. (A17a) and (A18b) are equal to Eqs. (A16a) and (A16c), respectively, and the sum of Eqs. (A17b) and (A18a) in the range of $\mu_1<x\le\pi-\mu_2$ is equal to Eq. (A16b). Eqs. (A17a)–(A17b) and (A18a)–(A18b) are regarded as dual series relations and by means of them, the coefficients C_0, D_0, C_n and D_n can be determined.

Eqs. (A17a) and (A17b) can be solved by the following procedure given in Sneddon ([22], p. 161). Assume that for $0\le x\le\mu_1$

$$\frac{1}{2}C_0+\sum_{n=1}^{\infty}C_n\cos(nx)=\cos\left(\frac{x}{2}\right)\int_x^{\mu_1}\frac{h_1(y)dy}{\sqrt{\cos x-\cos y}} \tag{A19}$$

where $h_1(y)$ is an unknown function to be determined. Using Eqs. (A17b) and (A19), for the full range $0\le x\le\pi$, the coefficients C_0 and C_n can then be expressed as ([22], (5.4.56), (5.4.57))

$$C_0=\frac{2}{\pi}\left[\frac{\pi}{\sqrt{2}}\int_0^{\mu_1}h_1(y)dy+\int_{\mu_1}^{\pi}\frac{1}{p}dy\right] \tag{A20}$$

and

$$C_n=\frac{2}{\pi}\left\{\frac{\pi}{2\sqrt{2}}\int_0^{\mu_1}h_1(y)[P_n(\cos y)+P_{n-1}(\cos y)]dy+\int_{\mu_1}^{\pi}\frac{1}{p}\cos(ny)dy\right\}. \tag{A21}$$

The function $h_1(y)$ can be determined using Eq. (A17a) for $0\le x\le\mu_1$. Integrating Eq. (A17a), one can obtain

$$\begin{aligned}&\frac{1}{2}C_0\sqrt{p}H(0,p)x+\sum_{n=1}^{\infty}C_n\sin(nx)\\&=\int_0^x\left[\sum_{n=1}^{\infty}C_nI_n\cos(nu)-\frac{1}{2}D_0\sqrt{p}H(0,p)-\sum_{n=1}^{\infty}D_n\lambda_nH_n\cos(nu)\right]du\\&=\int_0^xF(u)du\end{aligned} \tag{A22}$$

where $F(u)$ is defined as the integrand on the RHS of Eq. (A22). Substituting Eq. (A21) into Eq. (A22), one can find that $h_1(y)$ satisfies the following equation: ([22], p. 161, Eq. (5.4.58))

$$\begin{aligned}&\int_0^{\mu_1}h_1(y)\frac{1}{\sqrt{2}}\sum_{n=1}^{\infty}[P_n(\cos y)+P_{n-1}(\cos y)]\sin nxdy\\&=\int_0^xF(u)du-\frac{1}{2}\sqrt{p}H(0,p)C_0x-\sum_{n=1}^{\infty}\frac{2}{\pi}\int_{\mu_1}^{\pi}\frac{1}{p}\cos(nu)du\sin(nx).\end{aligned} \tag{A23}$$

The summation term on the left-hand side of Eq. (A23) can be expressed as ([22], p. 59, Eq. (2.6.31))

$$\frac{1}{\sqrt{2}}\sum_{n=1}^{\infty}[P_n(\cos y)+P_{n-1}(\cos y)]\sin nx=\frac{\cos\left(\frac{x}{2}\right)H_{eav}(x-y)}{\sqrt{\cos y-\cos x}} \tag{A24}$$

where $H_{eav}(X)$ is the Heaviside unit step function defined as

$$H_{eav}(X)=\begin{cases}0 & X<0\\1/2 & X=0\\1 & X>0\end{cases}. \tag{A25}$$

Substituting Eq. (A24) into Eq. (A23) yields

$$\begin{aligned}&\int_0^{\mu_1}\frac{h_1(y)H(x-y)}{\sqrt{\cos y-\cos x}}dy\\&=\sec\frac{x}{2}\left\{\int_0^xF(u)du-\frac{1}{2}\sqrt{p}H(0,p)C_0x-\sum_{n=1}^{\infty}\frac{2}{\pi}\int_{\mu_1}^{\pi}\frac{1}{p}\cos(nu)du\sin(nx)\right\}.\end{aligned} \tag{A26}$$

With Eq. (A25), Eq. (A26) can be expressed alternatively as

$$\begin{aligned}&\int_0^x\frac{h_1(y)}{\sqrt{\cos y-\cos x}}dy=\sec\frac{x}{2}\\&\times\left\{\int_0^xF(u)du-\frac{1}{2}\sqrt{p}H(0,p)C_0x-\sum_{n=1}^{\infty}\frac{2}{\pi}\int_{\mu_1}^{\pi}\frac{1}{p}\cos(nu)du\sin(nx)\right\}0\le x<\mu_1.\end{aligned} \tag{A27}$$

Then, the function $h_1(y)$ found based on Sneddon ([22], p. 162, Eq. (5.4.60)) is

$$\begin{aligned}h_1(y)=&\frac{2}{\pi}\frac{d}{dy}\int_0^y\frac{\sin(x/2)}{\sqrt{\cos x-\cos y}}\\&\times\left\{\int_0^xF(u)du-\frac{1}{2}\sqrt{p}H(0,p)C_0x-\sum_{n=1}^{\infty}\frac{2}{\pi}\int_{\mu_1}^{\pi}\frac{1}{p}\cos(nu)du\sin(nx)\right\}dx.\end{aligned} \tag{A28}$$

By integrating Eq. (A28) and substituting it into Eqs. (A20) and (A21), the coefficients C_0 and C_n can then be expressed as Eqs. (14) and (15), respectively.

For computational convenience, Eqs. (14) and (15) can be written as a vector equation

$$\mathbf{C}=(\mathbf{I}-\mathbf{X})^{-1}\mathbf{Y}\mathbf{D}+(\mathbf{I}-\mathbf{X})^{-1}\mathbf{Z} \tag{A29}$$

where $\mathbf{I}$ is an $(n+1)\times(n+1)$ identity matrix; $\mathbf{X}=[x_{i,j}]$ and $\mathbf{Y}=[y_{i,j}]$ are $(n+1)\times(n+1)$ matrices; $\mathbf{C}^T=[C_0, C_1,\ldots, C_n]$, $\mathbf{D}^T=[D_0, D_1,\ldots, D_n]$, and $\mathbf{Z}^T=[z_1, z_2,\ldots, z_{n+1}]$ are column vectors. The elements in the matrices and vectors are defined as

$$x_{1,1}=0 \tag{A30}$$

$$x_{1,j}=\frac{\frac{2}{(j-1)}I_{j-1}\Omega_2(\mu_1,j-1)}{1+\sqrt{p}H_0\Omega_1(\mu_1)} \tag{A31}$$

$$x_{ij}=\frac{1}{(j-1)}I_{j-1}\left[\Omega_2(\mu_1,j-1)f_2(i-1,\mu_1)-\int_0^{\mu_1}\Omega_2(y,j-1)\frac{df_2(i-1,y)}{dy}dy\right] \tag{A32}$$

$$x_{i1}=\frac{1}{2}\sqrt{p}H_0\left[\int_0^{\mu_2}\Omega_1(y)\frac{df_2(i-1,y)}{dy}dy-\Omega_1(\mu_1)f_2(i-1,\mu_1)\right] \tag{A33}$$

$$y_{11}=\frac{-\sqrt{p}H_0\Omega_1(\mu_1)}{1+\sqrt{p}H_0\Omega_1(\mu_1)} \tag{A34}$$

$$y_{1j} = \frac{\frac{-2}{(j-1)}\lambda_{j-1}H_{j-1}\Omega_2(\mu_1,j-1)}{1+\sqrt{p}H_0\Omega_1(\mu_1)} \tag{A35}$$

$$y_{i1} = \frac{1}{2}\sqrt{p}H_0\left[\int_0^{\mu_1}\Omega_1(y)\frac{df_2(i-1,y)}{dy}dy - \Omega_1(\mu_1)f_2(i-1,\mu_1)\right] \tag{A36}$$

$$y_{ij} = \frac{1}{(j-1)}\lambda_{j-1}H_{j-1}\left[\int_0^{\mu_1}\Omega_2(y,j-1)\frac{df_2(i-1,y)}{dy}dy - \Omega_2(\mu_1,j-1)f_2(i-1,\mu_1)\right] \tag{A37}$$

$$z_1 = \frac{\frac{4}{p\pi}\Omega_3(\mu_1)+\frac{2}{p}\left(1-\frac{\mu_1}{\pi}\right)}{1+\sqrt{p}H_0\Omega_1(\mu_1)} \tag{A38}$$

$$z_i = \frac{2}{p\pi}\left[\Omega_3(\mu_1)f_2(i-1,\mu_1) - \int_0^{\mu_1}\Omega_3(y)\frac{df_2(i-1,y)}{dy}dy\right] - \frac{2\sin((i-1)\mu_1)}{(i-1)\pi p} \tag{A39}$$

where i and j goes from 2 to n and the functions $f_1(\cdot)$, $f_2(\cdot)$ and $f_3(\cdot)$ are defined in Eqs. (25)–(27), respectively.

Similarly, Eqs. (A18a)–(A18b) can be solved by setting $x' = \pi - x$ and $D_n' = (-1)^n D_n$. Eqs. (A18a)–(A18b) is rewritten as

$$\frac{1}{2}D_0' + \sum_{n=1}^{\infty} D_n' \cos(nx') = 0, \qquad \mu_2 < x' \le \pi \tag{A40a}$$

$$\frac{1}{2}(D_0' + C_0)\sqrt{p}H_0 + \sum_{n=1}^{\infty}(D_n' + (-1)^n C_n)\lambda_n H_n \cos(nx') = 0, \quad 0 \le x' \le \mu_2 \tag{A40b}$$

and the vector equation for solving coefficients D_0 and D_n is expressed as

$$\mathbf{D} = \left(\mathbf{I} - \tilde{X}\right)^{-1}\tilde{Y}\mathbf{C} \tag{A41}$$

where $\tilde{X} = [\tilde{x}_{ij}]$ and $\tilde{Y} = [\tilde{y}_{ij}]$ are $(n+1)\times(n+1)$ matrices with the elements

$$\tilde{x}_{1,1} = 0 \tag{A42}$$

$$\tilde{x}_{1,j} = \frac{\frac{2(-1)^{j-1}}{(j-1)}I_{j-1}\Omega_2(\mu_2,j-1)}{1+\sqrt{p}H_0\Omega_1(\mu_2)} \tag{A43}$$

$$\tilde{x}_{i1} = \frac{1}{2}\sqrt{p}H_0\left[\int_0^{\mu_2}\Omega_1(y)\frac{df_2(i-1,y)}{dy}dy - \Omega_1(\mu_1)f_2(i-1,\mu_2)\right] \tag{A44}$$

$$\tilde{x}_{ij} = \frac{\sqrt{2}(-1)^{i-1}(-1)^{j-1}}{\pi(j-1)}I_{j-1}\left[\Omega_2(\mu_2,j-1)f_2(i-1,\mu_2) - \int_0^{\mu_2}\Omega_2(y,j-1)\frac{df_2(i-1,y)}{dy}dy\right] \tag{A45}$$

$$\tilde{y}_{11} = \frac{-\sqrt{p}H_0\Omega_1(\mu_2)}{1+\sqrt{p}H_0\Omega_1(\mu_2)} \tag{A46}$$

$$\tilde{y}_{1j} = \frac{\frac{-2(-1)^{j-1}}{(j-1)}\lambda_{j-1}H_{j-1}\Omega_2(\mu_2,j-1)}{1+\sqrt{p}H_0\Omega_1(\mu_2)} \tag{A47}$$

$$\tilde{y}_{i1} = \frac{(-1)^{i-1}}{2}\sqrt{p}H_0\left[\int_0^{\mu_2}\Omega_1(y)\frac{df_2(i-1,y)}{dy}dy - \Omega_1(\mu_2)f_2(i-1,\mu_2)\right] \tag{A48}$$

$$\tilde{y}_{ij} = \frac{(-1)^{j-1}(-1)^{i-1}}{(j-1)}\lambda_{j-1}H_{j-1} \times\left[\int_0^{\mu_2}\Omega_2(y,j-1)\frac{df_2(i-1,y)}{dy}dy - \Omega_2(\mu_2,j-1)f_2(i-1,\mu_2)\right]. \tag{A49}$$

If n tends to infinity, Eq. (11) would give the exact solution for the drawdown. However, it would give a relatively accurate result even a finite number of n is considered. Let n vary from 1 to N, where N is an arbitrary finite number. Substituting Eq. (A41) into Eq. (A29), the elements in **C** column vector can be expressed as

$$c_{j-1} = \sum_{i=1}^{N+1}\varphi_{i,j}z_i, j = 1,2,3,\ldots,N+1 \tag{A50}$$

with $\varphi_{i,j}$ represents (i,j)th element in the matrix $[\mathbf{I} - (\mathbf{I}-\mathbf{X})^{-1}\mathbf{Y}(\mathbf{I} - \tilde{X})^{-1}\tilde{Y}]^{-1}(\mathbf{I}-\mathbf{X})^{-1}$.

Once the coefficients C_0 and C_n are known, the coefficients D_0 and D_n can then be obtained from Eq. (A41).

References

[1] Abramowitz M, Stegun IA. Handbook of Mathematical Functions. New York: Dover Publications; 1970.
[2] Bassani JL, Nansteel MW, November M. Adiabatic-isothermal mixed boundary conditions in heat transfer. J Heat Mass Transfer 1987;30:903–9.
[3] Carslaw HS, Jaeger JC. Conduction of heat in solids. 2nd Ed. Oxford: Clarendon; 1959.
[4] Cassiani G, Kabala ZJ. Hydraulics of a partially penetrating well: solution to a mixed-type boundary value problem via dual integral equations. J Hydrol 1998;211:100–11.
[5] Cassiani G, Kabala ZJ, Medina Jr MA. Flowing partially penetrating well: solution to a mixed-type boundary value problem. Adv Water Resour 1999;23:59–68.
[6] Chang CC, Chen CS. An integral transform approach for a mixed boundary problem involving a flowing partially penetrating well with infinitesimal well skin. Water Resour Res 2002;38:1071.
[7] Chang CC, Chen CS. A flowing partially penetrating well in a finite-thickness aquifer: a mixed-type initial boundary value problem. J Hydrol 2003;271:101–18.
[8] Chang YC, Yeh HD. New solutions to the constant-head test performed at a partially penetrating well. J Hydrol 2009, doi:10.1016/j.jhydrol.2009.02.016.
[9] Chen YJ, Yeh HD. Parameter estimation/sensitivity analysis for an aquifer test with skin effect. Ground Water 2009;47:287–99, doi:10.1111/j.1745-6584.2008.00530.x.
[10] Gerald CF, Wheatley PO. Applied numerical analysis. 4th ed. California: Addison-Wesley; 1989.
[11] Hantush MS. Hydraulics of wells. In: Chow VT, editor. Advances in hydroscience, Vol. 1. New York: Academic Press; 1964.
[12] Huang SC, Chang YP. Anisotropic heat conduction with mixed boundary conditions. J Heat Transfer 1984;106:646–8.
[13] Huang SC. Unsteady-state heat conduction in semi-infinite regions with mixed-type boundary conditions. J Heat Transfer 1985;107:489–91.
[14] Huang YC, Yeh HD. The use of sensitivity analysis in on-line aquifer parameter estimation. J Hydrol 2007;335:406–18, doi:10.1016/j.jhydrol.2006.12.007.
[15] IMSL. Math/library, special functions. Houston: Visual Numerics Inc; 1997.
[16] Leng CH, Yeh HD. Aquifer parameter identification using the extended Kalman filter. Water Resour Res 2003;39:1062, doi:10.1029/2001WR000840.
[17] Lin YC, Yeh HD. Trihalomethane species forecast using optimization method: genetic algorithm and simulated annealing. Journal of Computing in Civil Engineering, ASCE 2005;19:248–57, doi:10.1061/(ASCE)0887-3801(2005)19:3(248).
[18] Noble B. Methods based on the Wiener–Hopf techniques. New York: Pergamon Press; 1958.
[19] Peng HY, Yeh HD, Yang SY. Improved numerical evaluation for the radial groundwater flow equation. Adv Water Resour 2002;25:663–75.
[20] Shanks D. Non-linear transformations of divergent and slowly convergent sequence. J Math Phys 1955;34:1–42.
[21] Selim MS, Kirkham D. Screen theory for wells and soil drainpipes. Water Resour Res 1974;10:1019–30.
[22] Sneddon IN. Mixed boundary value problems in potential theory. Amsterdam: North-Holland; 1966.
[23] Sneddon IN. The use of integral transforms. New York: McGraw-Hill; 1972. 540 pp.
[24] Stehfest, H., Algorithm 368, Numerical inversion of Laplace transforms, Comm. ACM, 13 (1 and 10) (1970), p. 47–49 and p.624.
[25] Wilkinson D, Hammond PS. A perturbation method for mixed boundary-value problems in pressure transient testing. Trans Porous Media 1990;5:609–36.
[26] Yang SY, Yeh HD. Solution for flow rates across the wellbore in a two-zone confined aquifer. J Hydraul Eng ASCE 2002;128:175–83.
[27] Yang SY, Yeh HD. Laplace-domain solutions for radial two-zone flow equations under the conditions of constant-head and partially penetrating well. J Hydraul Eng ASCE 2005;131:209–16.
[28] Yang SY, Yeh HD. An ovel analytical solution for constant-head test in a patchy aquifer. Int J Numer Anal Methods Geomech 2006;30:1213–30, doi:10.1002/nag.523.
[29] Yedder RB, Bilgen E. On adiabatic-isothermal mixed boundary conditions in heat transfer. Wärme Stoffübertragung 1994;29:457–60.
[30] Yeh HD. Theis' solution by nonlinear least-squares and finite-difference Newton's method. Ground Water 1987;25:710–5.
[31] Yeh HD, Han HY. Numerical identification of parameters in leaky aquifers. Ground Water 1989;27:655–63.
[32] Yeh HD, Chang TH, Lin YC. Groundwater contaminant source identification by a hybrid heuristic approach. Water Resour Res 2007;43:W09420, doi:10.1029/2005WR004731.

[33] Yeh HD, Huang YC. Parameter estimation for leaky aquifers using the extended Kalman filter and considering model and data measurement uncertainties. J Hydrol 2005;302:28–45, doi:10.1016/j.jhydrol.2004.06.035.
[34] Yeh HD, Yang SY, Peng HY. A new closed-form solution for a radial two-layer drawdown equation for groundwater under constant-flux pumping in a finite-radius well. Adv Water Res 2003;26:747–57.
[35] Yeh HD, Yang SY. A novel analytical solution for a slug test conducted in a well with a finite-thickness skin. Adv Water Resour 2006;29:1479–89, doi:10.1016/j.advwatres.2005.11.002.
[36] Zheng C, Bennett GD. Applied contaminant transport modeling. Second Edition. New York: Wiley; 2002. p. 621.